

Non-Hermitian quasicrystal in dimerized lattices

Longwen Zhou^{1,*} and Wenqian Han¹

¹*College of Physics and Optoelectronic Engineering,
Ocean University of China, Qingdao, China 266100*

(Dated: 2021-11-07)

Non-Hermitian quasicrystals possess \mathcal{PT} and metal-insulator transitions induced by gain and loss or nonreciprocal effects. In this work, we uncover the nature of localization transitions in a generalized Aubry-André-Harper model with dimerized hopping amplitudes and complex onsite potential. By investigating the spectrum, adjacent gap ratios and inverse participation ratios, we find an extended phase, a localized phase and a mobility edge phase, which are originated from the interplay between hopping dimerizations and non-Hermitian onsite potential. The lower and upper bounds of the mobility edge are further characterized by a pair of topological winding numbers, which undergo quantized jumps at the boundaries between different phases. Our discoveries thus unveil the richness of topological and transport phenomena in dimerized non-Hermitian quasicrystals.

I. INTRODUCTION

Quasicrystals have long-range order without spatial periodicity. They form a class of system in between crystals and fully disordered lattices [1–6]. Experimentally, quasicrystals have been realized in a variety of solid state materials and quantum simulators [7–13]. Rich phenomena induced by quasiperiodicity have been revealed, such as topological phases [14–21], quantized adiabatic pumping [15, 20, 21], anomalous transport and localization transitions [22–51], attracting attention over a broad range of research fields.

Recently, the study of quasicrystals has been extended to non-Hermitian systems, where the interplay between quasiperiodicity and gain/loss or nonreciprocity could induce exotic dynamical, localization and topological phenomena [52–69]. In particular, in non-Hermitian variants of the Aubry-André-Harper (AAH) model, complex onsite potential or nonreciprocal hopping could induce a \mathcal{PT} -breaking transition and a metal-insulator transition, which can be further characterized by a spectral topological winding number [52, 56]. In related studies, non-Hermiticity induced mobility edges in generalized and superconducting AAH models have also been found and described by topological invariants [54, 57–59, 62, 67]. Besides, the investigation of wavepacket spreading in non-Hermitian quasicrystals (NHQCs) have revealed their anomalous dynamical features [55, 60], such as the disordered-enhanced transport [55].

Meanwhile, the Su-Schrieffer-Heeger (SSH) model [70] provides another paradigm for the study of localization [71], topological [72] and non-Hermitian [73–75] physics. Specially, the hopping dimerization allows the SSH model to possess a topological phase characterized by an integer winding number and degenerate edge modes [72]. However, in the context of non-Hermitian quasicrystals, phases and phenomena that could arise due to the interplay between spatial aperiodicity and

hopping dimerization have not been revealed. In this manuscript, we address this issue by introducing a dimerized quasiperiodic lattice in Sec. II, which forms a hybridization of the SSH and non-Hermitian AAH models. The system is found to possess rich patterns of \mathcal{PT} -breaking and localization transitions, together with three phases of distinct transport nature. In Sec. III, we perform detailed analyses of the spectrum and localization nature of these phases, and construct a pair of topological winding numbers to characterize the transitions between them. Despite an extended and a localized phase, we also find a mobility edge phase, which is absent without the hopping dimerization. These discoveries thus uncover the richness of topological and transport phenomena in dimerized NHQCs. In Sec. IV, we summarize our results and discuss potential future directions. Further details about the spectrum, Lyapunov exponents and wavepacket dynamics are provided in the Appendixes A–C.

II. MODEL

In this section, we introduce the dimerized NHQC that will be investigated in this work. Our model can be viewed as an extension of the AAH model [5, 6], which is prototypical in the study of localization transitions in one-dimensional (1D) quasicrystals. In position representation, the Hamiltonian of the AAH model is $\hat{H}_{\text{AAH}} = \sum_n (J|n\rangle\langle n+1| + \text{H.c.} + V \cos(2\pi\alpha n + \lambda)|n\rangle\langle n|)$, where $\{|n\rangle\}$ represents the eigenbasis of the lattice, J is the hopping amplitude, V controls the strength of onsite potential, and λ is a phase shift. When α is irrational, the potential $V_n = V \cos(2\pi\alpha n + \lambda)$ is quasiperiodic in n , and \hat{H}_{AAH} describes a 1D quasicrystal. When $V < 2J$, the spectrum of \hat{H}_{AAH} is continuous and all its eigenstates are extended under the periodic boundary condition (PBC). Comparatively, \hat{H}_{AAH} possesses a point spectrum with localized eigenstates at all energies when $V > 2J$. When $V = 2J$, the spectrum of \hat{H}_{AAH} is purely singular continuous with critical wavefunctions,

* zhoulw13@u.nus.edu

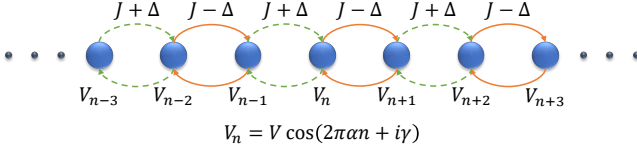


FIG. 1. Schematic illustration of the dimerized NHQC. Solid balls denote lattice sites with index $n \in \mathbb{Z}$. Hopping amplitudes are alternated between $J - \Delta$ (solid lines) and $J + \Delta$ (dashed lines). V_n represents the strength of onsite potential, with irrational modulation parameter α and phase shift $i\gamma$.

and the system undergoes a localization transition when V changes from $V < 2J$ to $V > 2J$ [4].

Recently, a non-Hermitian variant of \hat{H}_{AAH} was introduced by setting $\lambda = \beta + i\gamma$, with $(\beta, \gamma) \in \mathbb{R}$ [52]. Such a non-Hermitian AAH model possesses \mathcal{PT} -breaking and localization transitions at $\gamma_c = \ln(2J/V)$, which are accompanied by the quantized jump of a spectral winding number w . For $\gamma < \gamma_c$ ($\gamma > \gamma_c$), the spectrum is real (complex) with winding number $w = 0$ ($w = -1$), and each eigenstate is extended (localized) [52]. Since all states subject to the same localization transition at $\gamma = \gamma_c$, no mobility edges are found. Similar results are reported in a nonreciprocal AAH model [56], which might be related to the model in Ref. [52] by Fourier transformations.

In this work, we consider another extension of the AAH quasicrystal by introducing hopping dimerizations. We set $J \rightarrow J_n = J + (-1)^n \Delta$ as the hopping amplitude between the n 's and the $(n+1)$'s lattice sites, and let $\lambda = i\gamma$ be the imaginary phase shift in the onsite potential V_n . Our model Hamiltonian thus takes the form

$$\hat{H} = \sum_n \{ [J + (-1)^n \Delta] |n\rangle\langle n+1| + \text{H.c.} \} + \sum_n V \cos(2\pi\alpha n + i\gamma) |n\rangle\langle n|. \quad (1)$$

A schematic illustration of the model is shown in Fig. 1. When $V = 0$, Eq. (1) reduces to the SSH model with hopping dimerization Δ . With $V, \gamma \neq 0$, \hat{H} describes an SSH chain with quasiperiodically correlated non-Hermitian disorder. Therefore, our system realizes a hybridization between the AAH and SSH models. Since the realizations of SSH and non-Hermitian AAH models have both been discussed [52, 76], we expect our model to be within reach under current or near term experimental conditions. Furthermore, our construction allows us to explore the interplay between hopping dimerizations and quasiperiodic non-Hermitian potential, which could lead to rich phase diagrams and transport phenomena, as will be shown in the following section.

III. RESULTS

In this section, we investigate the dimerized NHQC in Eq. (1) from the perspective of spectrum, states, and topological invariants. In Sec. III A, we study the \mathcal{PT} -transitions in our system with respect to the hopping dimerization Δ and imaginary phase shift $i\gamma$. Adjacent gap ratios (AGRs) in the real part of the spectrum are found to exhibit three distinct regions of level statistics, implying the existence of an extended, a localized and a mobility edge phase in which extended and localized states coexist. In Sec. III B, we study the inverse participation ratios (IPRs) of the states in our system, and confirm the presence of a mobility edge region between the extended and localized phases in the parameter space, which is originated from the interplay between the dimerized hopping and complex onsite potential. Using the critical energies of the mobility edge, we construct a pair of topological winding numbers in Sec. III C, which could fully characterize the transitions between different phases. Throughout this section, we set the onsite modulation $\alpha = \frac{\sqrt{5}-1}{2}$ as the inverse of golden ratio to realize the quasiperiodicity of the potential. Under the PBC, we take the rational approximation of α by setting $\alpha \simeq p/q$, with p, q being two adjacent terms ($p < q$) in the Fibonacci sequence, and set the size of lattice $L = q$. We also let $J = 1$ be the unit of energy and set the Planck constant $\hbar = 1$. All system parameters are given in dimensionless units.

A. Spectrum and level statistics

The spectrum of the dimerized NHQC is obtained by solving the eigenvalue equation $\hat{H}|\psi\rangle = E|\psi\rangle$. Projecting the equation to the lattice representation, we find

$$[J + (-1)^n \Delta] \psi_{n+1} + [J + (-1)^{n-1} \Delta] \psi_{n-1} + V_n \psi_n = E \psi_n, \quad (2)$$

where $V_n = V \cos(2\pi\alpha n + i\gamma)$. Since $V_n = V_n^*$, \hat{H} possesses the \mathcal{PT} -symmetry and its spectrum can be real in the \mathcal{PT} -invariant region. With the increase of γ , one would expect a transition through which the \mathcal{PT} -symmetry is broken and the spectrum changes from real to complex. If $|\psi\rangle$ is an eigenstate of \hat{H} with energy E , $\mathcal{PT}|\psi\rangle$ should be an eigenstate with energy E^* . Therefore, the spectrum of \hat{H} is symmetric with respect to the real axis on the complex E plane. Furthermore, applying the chiral (sublattice) symmetry operator $\Gamma = \sum_n (-1)^{n-1} |n\rangle\langle n|$ to the eigenvalue equation, we obtain $\hat{H}'\Gamma|\psi\rangle = (-E)\Gamma|\psi\rangle$, where $\hat{H}' = \sum_n ([J + (-1)^n \Delta] |n\rangle\langle n+1| + \text{H.c.} + V \cos(2\pi\alpha n + \pi + i\gamma) |n\rangle\langle n|)$. Since α is irrational, $2\pi\alpha n \bmod 2\pi$ uniformly fills the range of $[0, 2\pi)$ for $n = 1, \dots, L$ in the thermodynamic limit $L \rightarrow \infty$. Therefore, it is possible to remove the extra phase shift π in \hat{H}' by resetting the origin of the lattice. \hat{H} and \hat{H}' thus share the same spec-

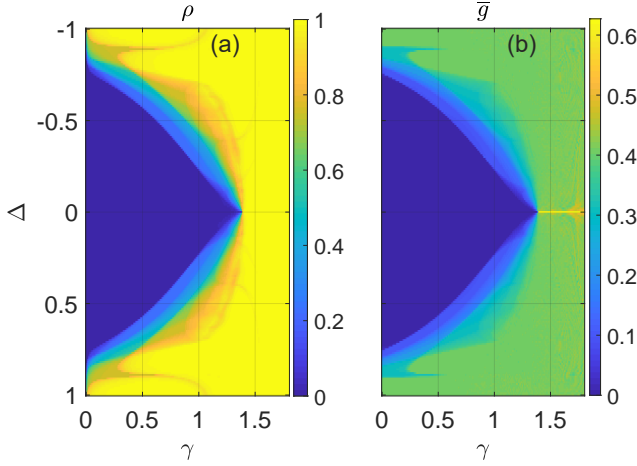


FIG. 2. Density of states with complex eigenvalues and averaged AGRs of \hat{H} versus the dimerization amplitude Δ and the imaginary part of phase shift γ in (a) and (b), respectively. System parameters are set as $J = 1$, $V = 0.5$, and $\alpha = \frac{\sqrt{5}-1}{2}$. PBC is taken in the calculation and the length of lattice is $L = 2584$.

trum in the limit $L \rightarrow \infty$. This implies that both E and $-E$ are eigenvalues of \hat{H} , and the spectrum of \hat{H} is symmetric with respect to the imaginary axis on the complex E plane. These generic features are confirmed by numerical results reported in Appendix A.

To have a comprehensive view of the spectrum and its connection with localization properties of states, we present the density of states with nonzero imaginary parts of energies and the mean of AGRs versus γ and Δ in Figs. 2(a) and 2(b), respectively. The density of states with complex energies is defined as

$$\rho \equiv \frac{1}{L} \sum_{j=1}^L N(|\text{Im}E_j|). \quad (3)$$

Here L is the length of lattice. For the j th eigenstate of \hat{H} with energy E_j , we have $N(|\text{Im}E_j|) = 1$ ($= 0$) if $|\text{Im}E_j| > 0$ ($|\text{Im}E_j| = 0$). The AGR is defined as $g_j \equiv \frac{\min(\epsilon_j, \epsilon_{j+1})}{\max(\epsilon_j, \epsilon_{j+1})}$, where $\epsilon_j = \text{Re}E_j - \text{Re}E_{j-1}$ denotes the spacing between the real parts of energies of the $(j-1)$'s and the j 's eigenstates of \hat{H} in ascending order. According to the non-Hermitian random-matrix theory [77–81], the statistical property of g_j is closely related to the localization features of non-Hermitian disordered systems. We consider the mean value of AGRs over all eigenstates [57], which is defined as

$$\bar{g} = \frac{1}{L} \sum_j g_j. \quad (4)$$

The values of \bar{g} in different parameter regions could provide us with a guideline to distinguish phases with distinct localization nature in the dimerized NHQC.

In Fig. 2(a), we find that all the eigenvalues of \hat{H} are real in a finite region (in dark blue) of the (γ, Δ) parameter space, in which $\rho = 0$ and the system is \mathcal{PT} -invariant. With the increase of γ and Δ , the spectrum changes from real to complex, with $0 < \rho < 1$, and the system enters a \mathcal{PT} -breaking phase. When γ is large enough, almost all states have complex eigenvalues and we have $\rho \simeq 1$. Notably, the boundary between the \mathcal{PT} -invariant and \mathcal{PT} -broken phases of the spectrum in Fig. 2(a) is consistent with the boundary separating states with averaged AGRs $\bar{g} \simeq 0$ and $\bar{g} > 0$ in Fig. 2(b). According to the general results of level statistics, all eigenstates of \hat{H} would be extended when $\bar{g} \simeq 0$. Therefore, we expect an extended phase in the \mathcal{PT} -invariant region of \hat{H} . Moreover, the region with $\bar{g} > 0$ in Fig. 2(b) can be separated into two distinct zones. When γ is large enough, we find $\bar{g} \simeq 0.4$ for all γ with $\Delta \neq 0$, which corresponds to a localized phase according to the level statistics [77–81]. In the region with $0 < \bar{g} < 0.4$, \bar{g} grows smoothly with the increase of γ and Δ , implying the existence of a mobility edge phase. The emergence of such a phase is solely due to the hopping dimerization, which is absent in the original AAH model. These observations are further confirmed by the study of IPRs presented in the next subsection.

B. Inverse participation ratio

To further unveil the localization nature of states in the dimerized NHQC, we study the IPR of our system in this subsection. For a normalized eigenstate $|\psi^{(j)}\rangle = \sum_n \psi_n^{(j)} |n\rangle$ of \hat{H} , the IPR is defined in the lattice representation as $\text{IPR}^{(j)} \equiv \sum_{n=1}^L |\psi_n^{(j)}|^4$, where L is the length of lattice. For 1D systems in the thermodynamic limit, we generally have $\text{IPR} \sim L^{-1}$ if $|\psi\rangle$ is an extended state, and $\text{IPR} \sim \xi^{-1}$ if $|\psi\rangle$ is localized, where the localization length ξ is independent of L [82]. Therefore, we expect that when L is large, all the eigenstates of \hat{H} have $\text{IPR} \simeq 0$ in the extended phase. To capture the localization transitions between different phases, we further introduce the maximum and minimum of IPRs, which are defined as

$$\max(\text{IPR}) \equiv \max_{j \in \{1, \dots, L\}} \text{IPR}^{(j)}, \quad (5)$$

$$\min(\text{IPR}) \equiv \min_{j \in \{1, \dots, L\}} \text{IPR}^{(j)}. \quad (6)$$

When $\max(\text{IPR})$ diverges from zero but $\min(\text{IPR})$ remains at zero, localized states start to appear and the system switches from the extended to the mobility edge phase. When $\min(\text{IPR})$ also deviates from zero, the last extended state vanishes and the system enters a phase in which all states are localized. The maximal and minimal values of IPR can thus be used to distinguish phases with different localization nature and locate the corresponding phase boundaries.

In Fig. 3, we present the maximum and minimum

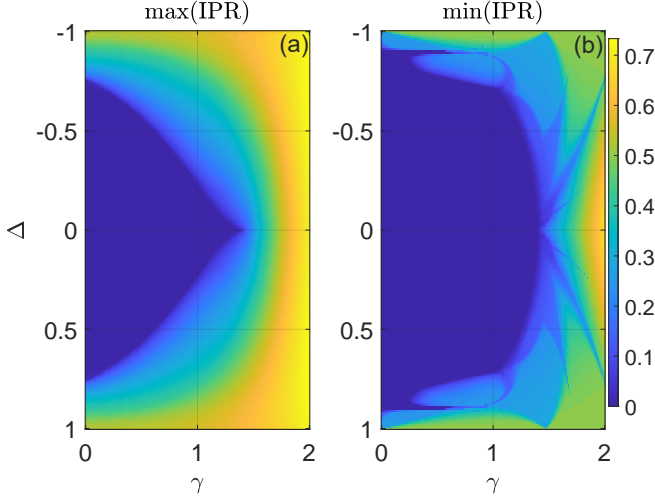


FIG. 3. The maximum and minimum of IPRs versus the imaginary part of phase shift γ and hopping dimerization Δ in (a) and (b). System parameters are set as $J = 1$, $V = 0.5$, and $\alpha = \frac{\sqrt{5}-1}{2}$. The length of lattice is $L = 610$. PBC is taken in the diagonalization \hat{H} .

of IPRs versus the imaginary phase shift and hopping dimerization. In Fig. 3(a), we find a region with $\max(\text{IPR}) \simeq 0$ (in dark blue) in the γ - Δ parameter space, which means that all states of \hat{H} for a given set of system parameters in this region are extended. Notably, the scope of this region is coincide with the regions in Fig. 2, in which the density of states ρ and averaged AGRs \bar{g} vanish. Therefore, the domain with $\max(\text{IPR}) \simeq 0$ indeed corresponds to a \mathcal{PT} -invariant extended phase, in which all eigenstates of \hat{H} have real energies and delocalized profiles. In Fig. 3(b), we also observe a zone with $\min(\text{IPR}) \simeq 0$ (in dark blue), in which extended eigenstates of \hat{H} persist up to its boundary. As expected, the zone with $\min(\text{IPR}) \simeq 0$ covers the region with $\max(\text{IPR}) \simeq 0$. Beyond that, we have an intermediate region with $\min(\text{IPR}) \simeq 0$ and $\max(\text{IPR}) > 0$, before the system enters a localized phase with $\min(\text{IPR}) > 0$. In the intermediate region, since there are states with both vanishing and finite IPRs, extended and localized states must coexist. The range of this intermediate region is also consistent with the regions in Fig. 2 with $0 < \rho < 1$ and $0 < \bar{g} < 0.4$. These observations confirm that there indeed exists a mobility edge phase between the extended and localized phases of the dimerized NHQC, in which the \mathcal{PT} -symmetry is broken and yet only part of the states are localized with complex energies. Note that this mobility edge phase does not exist in the non-Hermitian AAH model with $\Delta = 0$, which highlights the importance of hopping dimerizations in creating unique states of matter and localization transitions in non-Hermitian quasicrystals.

To summarize, we find that the IPR can be viewed as an “order parameter” to describe the localization transitions in the dimerized NHQC. The behaviors of IPRs in

distinct parameter domains could be employed to characterize the three different phases in the system. For completeness, we study the Lyapunov exponents of the system in Appendix B, and find consistent results as predicted by IPRs. We have also checked the spectrum and IPRs of the system under the open boundary condition (OBC), and find consistent results with those obtained under the PBC, excluding possible impact of non-Hermitian skin effects. In the following, we demonstrate that the localization transitions in our system are of topological origin, and can be depicted by a pair of spectral winding numbers.

C. Topological winding number

In previous studies, spectral winding numbers have been employed to characterize non-Hermitian topological matter in 1D clean and disordered systems [52, 73]. For the dimerized NHQC, we can introduce a pair of winding numbers to describe the topological nature of its localization transitions. These numbers can be defined as

$$w_\ell = \lim_{N \rightarrow \infty} \frac{1}{2\pi i} \int_0^{2\pi} d\beta \partial_\beta \ln \{ \det [H(\beta/N) - \mathcal{E}_\ell] \}. \quad (7)$$

N is the number of dimerized cells of the lattice and $\ell = 1, 2$. The phase shift β/N is introduced into the Hamiltonian \hat{H} via setting $V_n \rightarrow V \cos(2\pi\alpha n + \beta/N + i\gamma)$. $(\mathcal{E}_1, \mathcal{E}_2)$ are two real-valued base energies, and (w_1, w_2) count the number of times the spectrum of $H(\beta/N)$ winds around these energies when β sweeps over a cycle from zero to 2π . It is clear that w_1 (w_2) can be nonzero only if the spectrum of \hat{H} around \mathcal{E}_1 (\mathcal{E}_2) take complex values. These winding numbers are thus closely related to the complex spectrum structure of the system. When the spectral does not possess a mobility edge, there is only a single base energy that can in principle be chosen arbitrarily [52], and we would always have $w_1 = w_2$. In our model this is the case when $\Delta = 0$ (uniform hopping). If mobility edges exist in the spectral, the choice of base energies $(\mathcal{E}_1, \mathcal{E}_2)$ should be related to its boundaries [54]. More precisely, in a given range of imaginary phase shift $i\gamma$ or hopping dimerization Δ , we choose \mathcal{E}_1 to be the real part of energy of the first eigenstate of \hat{H} whose IPR starts to deviate from zero, i.e., the first eigenstate that becomes localized. Similarly, we set \mathcal{E}_2 as the real part of energy of the last eigenstate whose profile changes from extended to localized. \mathcal{E}_1 and \mathcal{E}_2 thus decide the lower and upper bounds of the mobility edge on the $\text{Re}E$ - γ or $\text{Re}E$ - Δ plane. The winding numbers w_1 and w_2 defined with respect to \mathcal{E}_1 and \mathcal{E}_2 are expected to have quantized jumps when the mobility edge appears and vanishes in the spectrum [54].

In Fig. 4, we report the winding numbers, the maximal imaginary parts of energy, the averaged AGRs and the IPRs together for a typical set of system parameters. We find that the invariants $(w_1, w_2) = (0, 0)$ in

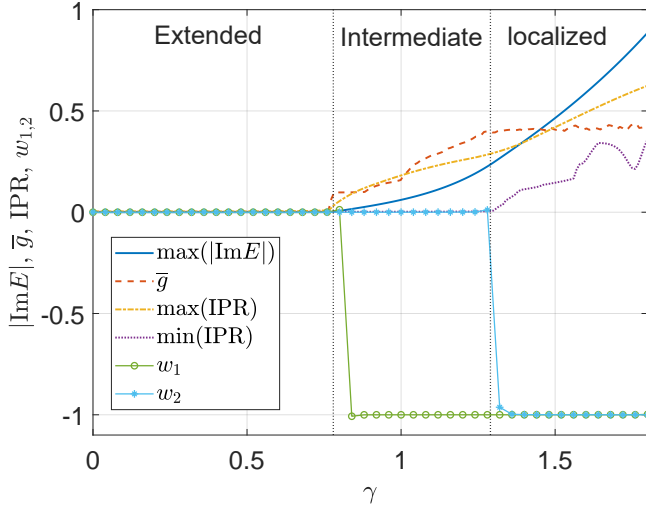


FIG. 4. The winding numbers (w_1, w_2) versus the imaginary part of phase shift γ . System parameters are set as $J = 1$, $V = 0.5$, $\Delta = 0.4$, $\alpha = \frac{\sqrt{5}-1}{2}$. The size of lattice is $L = 610$ with PBC. The vertical dotted lines highlight the critical values γ_{c1} and γ_{c2} , where transitions between different phases happen.

the \mathcal{PT} -invariant extended phase, with $\max(|\text{Im}E|) \simeq \bar{g} \simeq \max(\text{IPR}) \simeq \min(\text{IPR}) = 0$. When the imaginary part of phase shift passes the first critical point $\gamma_{c1} \approx 0.78$, w_1 undergoes a quantized jump from 0 to -1 , and $[\bar{g}, \max(\text{IPR})]$ start to deviate from zero. The system thus enters a mobility edge phase with winding numbers $(w_1, w_2) = (-1, 0)$. Note that such a phase is absent if $\Delta = 0$, which reveals the role of hopping dimerization in the creating of new phases and phase transitions in the dimerized NHQC. When γ goes through the second critical point $\gamma_{c2} \approx 1.29$, the winding number w_1 stays at -1 while w_2 jumps from zero to -1 . Meanwhile, $\min(\text{IPR})$ starts to deviate from zero and the averaged AGR converges to $\bar{g} \simeq 0.4$. The system therefore gets into a phase with localized eigenstates at all possible energies and winding numbers $(w_1, w_2) = (-1, -1)$. The invariants (w_1, w_2) can thus be used to distinguish the three possible phases with different localization nature in the system, and characterize the transitions between them.

In Fig. 5, we present the topological phase diagrams of the dimerized NHQC versus the imaginary part of phase shift and hopping dimerization for two typical sets of system parameters. In the region of $\rho \simeq 0$ [real spectrum, see also Fig. 2(a)] and $\max(\text{IPR}) \simeq 0$ [all bulk states are extended, see also Fig. 3(a)], we find $w_1 = w_2 = 0$, implying that the \mathcal{PT} -invariant extended phase is topologically trivial according to the spectral winding numbers. When ρ and $\max(\text{IPR})$ start to deviate from zero, the system undergoes a \mathcal{PT} -breaking transition and enters a mobility edge phase. In the meantime, w_1 takes a quantized jump from 0 to -1 , whereas w_2 remains at zero in Fig. 5(a). The transition from extended to mo-

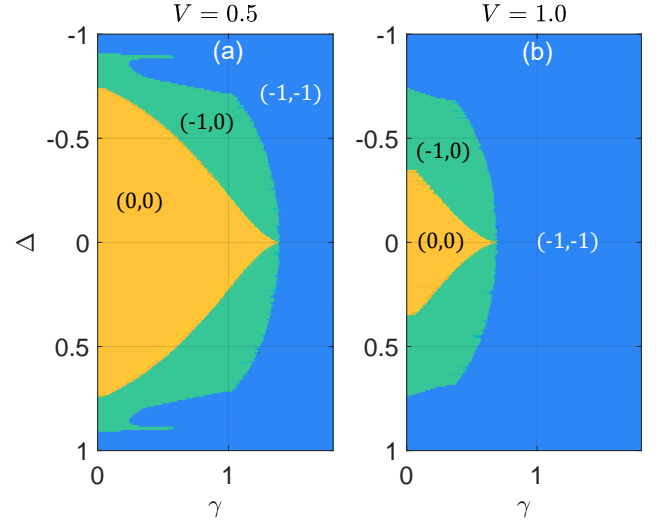


FIG. 5. Topological phase diagrams of the dimerized NHQC. System parameters are set as $J = 1$, $\alpha = \frac{\sqrt{5}-1}{2}$, and $V = 0.5$ ($V = 1$) for (a) [(b)]. The length of lattice is $L = 610$, containing $N = 305$ dimerized cells. In (a) and (b), each region with a uniform color corresponds to a topological phase, whose winding numbers are denoted therein. The extended, mobility edge and localized phases have $(w_1, w_2) = (0, 0)$, $(-1, 0)$ and $(-1, -1)$. w_1 or w_2 jumps at a boundary between different phases. PBC is taken in the calculation.

bility edge phases is thus topological and captured by the quantized change of winding number w_1 . The mobility edge phase can also be viewed as a topological phase characterized by $(w_1, w_2) = (-1, 0)$. When $\rho \simeq 1$ and $\min(\text{IPR})$ starts to deviate from zero, the system enters a localized phase and all bulk states take complex eigenvalues. Meanwhile, the winding number w_2 jumps from 0 to -1 whereas w_1 remains at -1 , as shown in Fig. 5(a). Therefore, the transition from the mobility edge to localized phases is also topological and accompanied by the quantized change of winding number w_2 by -1 . The localized phase can then be viewed as a topological phase with $(w_1, w_2) = (-1, -1)$. These observations are all demonstrated in the phase diagram Fig. 5(a). We also considered other possible amplitudes of onsite potential V [with one example given in Fig. 5(b)], and obtain similar kinds of diagrams, which verifies the generality of our approach to the characterization of localization transitions and topological phases in dimerized NHQCs. We summarize the key results of this section in Table I.

IV. DISCUSSION

In experiments, the dimerized NHQC might be engineered in photonic systems. The uniform part of hopping amplitude and non-Hermitian quasiperiodic potential could be realized by a frequency-modulated mode-locked laser with gain medium, phase modulator and low-finesse intracavity etalon, as proposed in Ref. [52].

Phase	Extended	Mobility Edge	Localized
Spectrum	Real	Complex	
Averaged AGR	$\bar{g} \simeq 0$	$0 < \bar{g} < 0.4$	$\bar{g} \simeq 0.4$
IPR	$\simeq 0$ for all states	> 0 & $\simeq 0$ coexist	> 0 for all states
Winding number	$(w_1, w_2) = (0, 0)$	$(w_1, w_2) = (-1, 0)$	$(w_1, w_2) = (-1, -1)$

TABLE I. Summary of the results for the dimerized NHQC.

The dimerized hopping amplitude could be realized by engineering the profile of refractive index in the model-locked laser setup [76]. Therefore, our model should be within reach in current or near-term experimental situations. To promote the detection and characterization of different phases in the dimerized NHQC, we also investigate its wavepacket dynamics in Appendix C, and find connections between the dynamical signatures and localization properties of the system.

In conclusion, we find localization and topological transitions in a dimerized NHQC, which are originated from the cooperation between hopping dimerizations and complex onsite quasiperiodic potential. In the region of weak dimerization and non-Hermiticity, the system is in an extended phase with real spectrum and delocalized eigenstates. With the increase of hopping dimerization and complex potential, the system transforms into a mobility edge phase. When the strength of hopping dimerization and non-Hermitian modulation become stronger, the system enters a third phase in which the spectrum is complex and all eigenstates are localized. Moreover, the transitions between the extended, mobility edge and localized phases are of topological nature. They can be characterized by the quantized jumps of two spectral winding numbers. Our results thus uncover the unique spectrum, topological and transport features of quasicrystals due to the interplay between hopping dimerizations and non-Hermitian onsite potential. The different phases and transitions found in our system further reveal the richness of localization and topological phenomena in non-Hermitian quasicrystals. In future work, it would be interesting to consider the impact of hopping dimerizations in other types of nonreciprocal and non-Hermitian quasicrystals, and explore the effect of nonlinearity, many-body interactions and skin effects on the localization and topological physics in dimerized non-Hermitian systems.

ACKNOWLEDGMENTS

This work is supported by the National Natural Science Foundation of China (Grant No. 11905211), the China Postdoctoral Science Foundation (Grant No. 2019M662444), the Fundamental Research Funds for the Central Universities (Grant No. 841912009), the Young Talents Project at Ocean University of China (Grant No. 861801013196), and the Applied Research Project of Postdoctoral Fellows in Qingdao (Grant No. 861905040009).

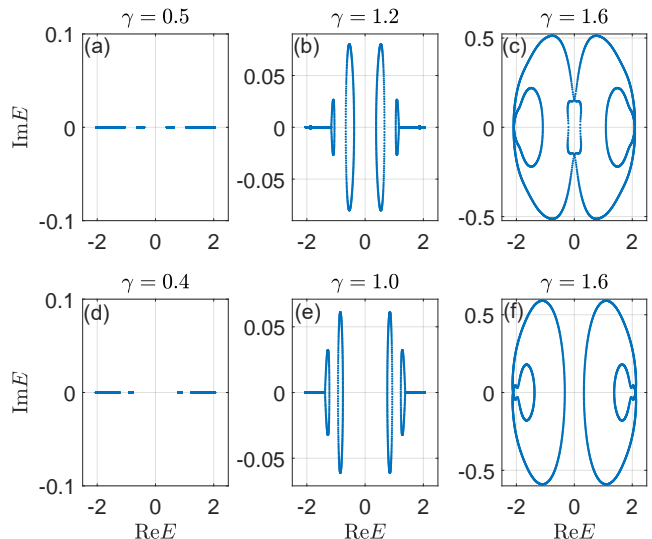


FIG. 6. The spectrum of the dimerized NHQC model under PBC on the complex plane. System parameters are set as $J = 1$, $V = 0.5$, $\alpha = \frac{\sqrt{5}-1}{2}$, and $\Delta = 0.2$ ($\Delta = 0.4$) for (a)–(c) [(d)–(f)]. The values of the imaginary part of phase shift are shown in the captions. The length of lattice is $L = 2584$.

Appendix A: Detail of the spectrum

In this appendix, we provide more details about the spectrum of the dimerized NHQC. In Fig. 6, we present the spectrum for a typical set of system parameters. When the imaginary part of phase shift γ is small, we observe real spectrum in Figs. 6(a) and 6(d), implying that the system is in the \mathcal{PT} -invariant region. With the increase of γ , the spectrum starts to become complex and developing loops on the complex E plane, which means that the system has undergone a \mathcal{PT} -transition and roamed into a \mathcal{PT} -broken region. However, parts of the spectrum are still pinned to the real axis in Figs. 6(b) and 6(e), indicating that the eigenstates with real and complex eigenvalues coexist in these cases. When γ further increases, the number of eigenstates with real eigenvalues tends to decrease, and finally almost all states have complex energies, as shown in Figs. 6(c) and 6(f). Besides, the range and shape of spectrum also depend on the dimerization strength Δ , which reveals that both the hopping dimerization and complex onsite potential could affect the properties of the spectrum.

Appendix B: Lyapunov exponent

In this appendix, we investigate the Lyapunov exponent (LE) of the dimerized NHQC, and compare it with the results deduced from IPRs in the main text. The LE is the inverse of localization length, which in the thermodynamic limit approaches zero for an extended state, and taking a finite value for a localized state. For an eigenstate $|\psi^{(j)}\rangle = \sum_n \psi_n^{(j)} |n\rangle$ of \hat{H} with energy E_j , the LE is defined in the lattice representation as $\zeta_j = -\lim_{L \rightarrow \infty} \frac{1}{L} \ln |\psi_L^{(j)} / \psi_1^{(j)}|$. Under the OBC, the \hat{H} in Eq. (1) takes a tridiagonal form in the lattice representation, and ζ_j can be expressed by eigenenergies [53], i.e.,

$$\zeta_j = \lim_{L \rightarrow \infty} \frac{1}{L} \left(\sum_{n=1, n \neq j}^L \ln |E_j - E_n| - \sum_{n=1}^{L-1} \ln |t_n| \right), \quad (\text{B1})$$

where $t_n = J + (-1)^n \Delta$ is the dimerized hopping amplitude. When the minimum of ζ_j , i.e.,

$$\zeta_{\min} \equiv \lim_{L \rightarrow \infty} \left(\min_{j \in \{1, \dots, L\}} \zeta_j \right), \quad (\text{B2})$$

starts to deviate appreciably from zero, we expect all eigenstates to become localized and the system enters an insulator phase. ζ_{\min} can thus be utilized to determine the onset of a fully localized phase, just like the $\min(\text{IPR})$ in the main text. However, due to the existence of edge states under the OBC, one cannot directly extract the boundary contour between extended and mobility edge phases from the maximum of LEs, since the LE of edge states are always nonzero even when all bulk states are extended. To resolve this issue, we consider the LE after taking the average over all bulk and edge states, which is defined as $\zeta_{\text{ave}} = \lim_{L \rightarrow \infty} \frac{1}{L} \sum_{j=1}^L \zeta_j$. Since the number of edge states is significantly smaller than the bulk states, we expect $\zeta_{\text{ave}} \rightarrow 0$ in the thermodynamic limit if all bulk states are extended, and $\zeta_{\text{ave}} > 0$ when a sufficient number of bulk states ($\propto L$) become localized. ζ_{ave} can thus be employed to locate the boundary between the extended and mobility edge phases. To show the boundary contour separating these two phases more clearly, we evaluate the partial derivative

$$\zeta'_{\text{ave}} \equiv \partial_\gamma \zeta_{\text{ave}}. \quad (\text{B3})$$

In the bulk extended phase, the number of edge states is a constant for a given L , and we expect $\zeta'_{\text{ave}} = 0$. Beyond the extended phase, localized bulk states appear and their number increases with γ , yielding $\zeta'_{\text{ave}} > 0$. The boundary between the regions with $\zeta'_{\text{ave}} = 0$ and $\zeta'_{\text{ave}} > 0$ should thus correspond to the boundary between extended and mobility edge phases of the system.

In Fig. 7, we show the IPRs and LEs versus the imaginary part of phase shift at different hopping dimerizations. We observe that when Δ is small, the $\max(\text{IPR})$,

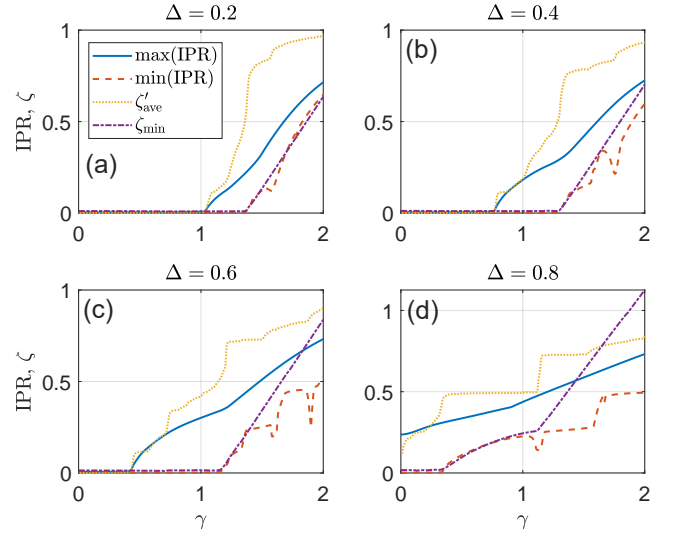


FIG. 7. IPRs and LEs versus the imaginary part of phase shift γ . System parameters are $J = 1$, $V = 0.5$, and $\alpha = \frac{\sqrt{5}-1}{2}$. The length of lattice is $L = 610$, and PBC (OBC) is taken in the calculation of IPRs (LEs). In (a)–(d), the solid (dashed) lines represent the maximum (minimum) of IPRs and the dotted (dash-dotted) lines show the derivative of averaged (minimum of) LE.

$\min(\text{IPR})$, ζ'_{ave} and ζ_{\min} are all pinned to zero over a range of γ . Compared with the results reported in Fig. 2, it can be verified that the spectrum of the system is real in this region. Therefore, if $\max(\text{IPR}) \simeq \min(\text{IPR}) \simeq \zeta'_{\text{ave}} \simeq \zeta_{\min} \simeq 0$, our system is in a \mathcal{PT} -invariant extended phase. When γ exceeds certain critical point γ_{c1} , both the $\max(\text{IPR})$ and ζ'_{ave} start to deviate from zero, even though the $\min(\text{IPR})$ and ζ_{\min} are still stuck to zero. Typical forms of spectrum of the system in this region are shown in Figs. 6(b) and 6(e). Referring to Fig. 2, it can be checked that the region with $\max(\text{IPR}) > 0$, $\zeta'_{\text{ave}} > 0$ and $\min(\text{IPR}) \simeq \zeta_{\min} \simeq 0$ also has $0 < \rho < 1$ and $0 < \bar{g} < 0.4$. The system is therefore in a mobility edge phase in this region. When γ further increases and goes beyond a second critical point γ_{c2} , the $\max(\text{IPR})$, $\min(\text{IPR})$, ζ'_{ave} and ζ_{\min} all deviate from zero. According to Fig. 2, the system has $\rho \simeq 1$ and $\bar{g} \simeq 0.4$ in this region. It thus enters an insulator phase in which all bulk states have complex energies. Note that in Figs. 7(a)–(c), the range of the mobility edge phase and the critical values γ_{c1}, γ_{c2} are all affected by the hopping dimerization Δ . Moreover, the extended phase could vanish when Δ is large enough, as shown in Fig. 7(d), where we have $\max(\text{IPR}) > 0$, $\zeta'_{\text{ave}} > 0$ from the very beginning. Therefore, both the hopping dimerization and onsite complex potential control the localization transitions in the dimerized NHQC, and their interplay determines the complete phase diagram of the system.

In Fig. 8, we present the LEs versus the imaginary part of phase shift and hopping dimerization. In Fig. 8(a), we find a region with $\zeta'_{\text{ave}} \simeq 0$ (in dark blue) in the parameter

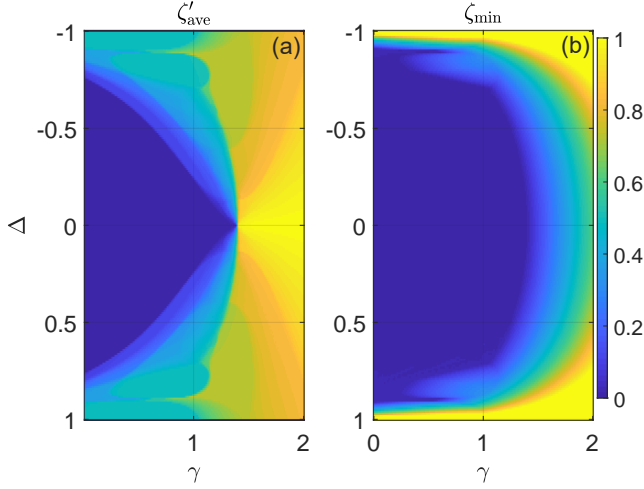


FIG. 8. The minimum and derivative of LEs, as defined in Eqs. (B2) and (B3), versus the imaginary part of phase shift γ and hopping dimerization Δ . System parameters are set as $J = 1$, $V = 0.5$, and $\alpha = \frac{\sqrt{5}-1}{2}$. The length of lattice is $L = 610$ and the OBC is taken in the diagonalization \hat{H} .

space, meaning that all states of \hat{H} therein are extended. Notably, the scope of this region is coincide with the region of Fig. 3(a) with $\max(\text{IPR}) \simeq 0$, and also the regions in Fig. 2 where the density of states with complex eigenvalues and averaged AGR vanish. Therefore, the region with $\zeta'_{ave} \simeq 0$ in Fig. 8(a) corresponds to a \mathcal{PT} -invariant extended phase, in which all eigenstates of \hat{H} have real energies. In Fig. 8(b), we observe a zone with $\zeta_{min} \simeq 0$ (in dark blue), in which extended states of \hat{H} persist up to its boundary. The zone with $\zeta_{min} \simeq 0$ covers the region with $\zeta'_{ave} \simeq 0$. Beyond that, we find a region with $\zeta_{min} \simeq 0$ and $\zeta'_{ave} > 0$ before the system entering a localized phase. The scope of this region is consistent with the region in Fig. 3 with $\min(\text{IPR}) \simeq 0$, $\max(\text{IPR}) > 0$, and with the region in Fig. 2 with $0 < \rho < 1$, $0 < \bar{g} < 0.4$, verifying that there indeed exists a mobility edge phase in the dimerized NHQC.

Appendix C: Wavepacket dynamics

In this appendix, we investigate the dynamical properties of the dimerized NHQC, and suggest to characterize the different phases by the spreading velocity and return probability of wavepackets. The evolution of a state in our system is obtained by solving the time-dependent Schrödinger equation, yielding $|\tilde{\psi}(t)\rangle = e^{-i\hat{H}t}|\psi(0)\rangle$. Since \hat{H} is non-Hermitian, the evolution can be nonunitary and the state $|\tilde{\psi}(t)\rangle$ is not normalized. The normalized state is given by $|\psi(t)\rangle = |\tilde{\psi}(t)\rangle / \sqrt{\langle \tilde{\psi}(t) | \tilde{\psi}(t) \rangle}$, which can be used to study the probability distribution and expectation values of observables. To characterize the spreading of a wavepacket, we consider its sec-

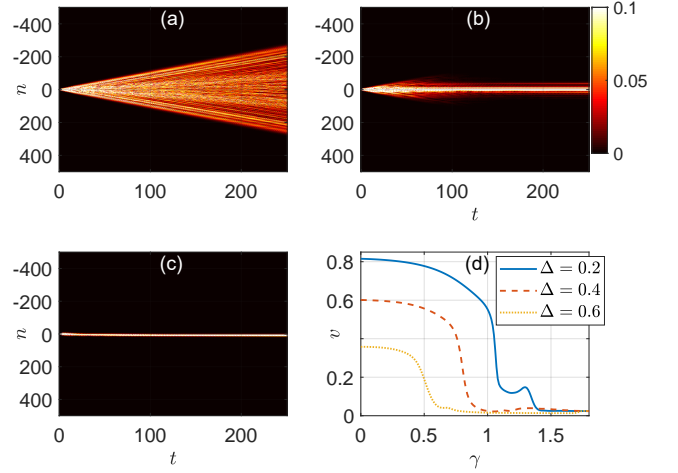


FIG. 9. Profiles (a)–(c) and spreading velocities (d) of wavepackets initially localized at the central site of the lattice. The imaginary phase shift is set as (a) $\gamma = 0.4$, (b) $\gamma = 1$ and (c) $\gamma = 1.6$. System parameters are $J = 1$, $V = 0.5$, $\Delta = 0.4$ in (a)–(c). The length of lattice is $L = 1000$ with PBC. The spreading velocity v is obtained in (d) after averaging $v(t)$ over a time span of $t = 250$.

ond moment, which in the lattice representation reads $\sigma_2 = \sum_{n=1}^L n^2 |\psi_n(t)|^2$. Here n is the lattice index and $\psi_n(t) = \langle n | \psi(t) \rangle$. From the second moment, we can further obtain the spreading velocity of the wavepacket by averaging over a time duration [55], i.e., $v(t) = \sqrt{\sigma_2}/t$, which could behave differently if the wavepacket is initialized in different phases of the system. In the extended phase, an initially localized wavepacket is expected to undergo ballistic spreading, forming a light cone pattern on the space-time plane if the hopping is symmetric [55]. The velocity $v(t)$ of the wavepacket would be finite. In an insulator phase, an initially localized wavepacket will refuse to spread and stay around its original site. Its spreading velocity $v(t)$ will also vanish, showing the phenomena of dynamical localization [55].

In Fig. 9, we show the profiles of wavepacket during the evolution and the averaged spreading velocity for a typical set of system parameters. In Fig. 9(a), the system is set in the extended phase (see also Fig. 4). We observe that the wavepacket indeed performs a ballistic spreading and presents a light cone pattern. In Fig. 9(b), the system is set in the mobility edge phase (see also Fig. 4). The wavepacket is initially found to undergo a slow spreading over a finite range of sites. At a later stage, the spreading tends to terminate and the wavepacket retains a finite width around its original site. The initial spreading process may be assisted by the remaining extended states of the mobility edge phase. But during the evolution, the wavepacket develops more overlap with the localized states, which finally help to shut off its transport in the lattice. In Fig. 9(c), the parameters of \hat{H} are set in the localized phase (see also Fig. 4). As expected, the wavepacket could not spread and remains exponen-

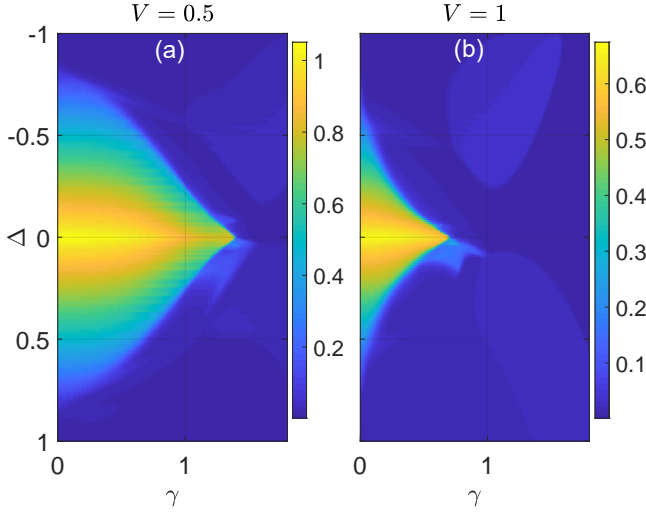


FIG. 10. Spreading velocities of an initially localized wavepacket versus the imaginary part of phase shift γ and hopping dimerization Δ . $v(t)$ is averaged over a time duration $t = 250$. The strength of the onsite potential is $V = 0.5$ in (a) and $V = 1$ in (b). System parameters are set as $J = 1$ and $\alpha = \frac{\sqrt{5}-1}{2}$. The length of lattice is $L = 1000$ with PBC, and the initial state satisfies $\langle n | \psi(0) \rangle = \delta_{n0}$.

tially localized around its original location. The distinctive signatures of wavepacket spreading in these three phases could then provide us with a dynamical way of distinguishing them. In Fig. 9(d), the spreading velocity of a wavepacket is found to decrease with the increase of γ when the system is set in the extended phase. At large γ , the system enters the localized phase and the velocity approaches zero. When γ goes across the boundary between the extended and mobility edge phases, the velocity shows a quick drop in a small range of γ , implying the appearance of a dynamical transition between these two phases. Notably, the critical point γ_{c1} of the transition is different for different hopping dimerizations, and the velocity could also show an anomalous growth with the increase of γ in the mobility edge phase [e.g., see the solid line in Fig. 9(d)]. These observations suggest that the interplay between hopping dimerizations and complex onsite potential could not only create new types of dynamical phases in non-Hermitian quasicrystals, but also cause non-Hermiticity enhanced transport observed previously in systems with nonreciprocal hopping [55].

In Fig. 10, we plot the mean velocities of initially localized wavepackets versus the imaginary part of phase shift and hopping dimerization. In Figs. 10(a) and 10(b), we find clear borders between regions in which v take finite values and approaches zero. They coincide with the boundaries between extended and mobility edge phases, as shown in Figs. 5(a) and 5(b). Therefore, the velocity of wavepackets could be employed to locate the boundaries between extended and mobility edge phases. However, we could not observe a clear dynamical signature of the boundary between mobility edge and local-

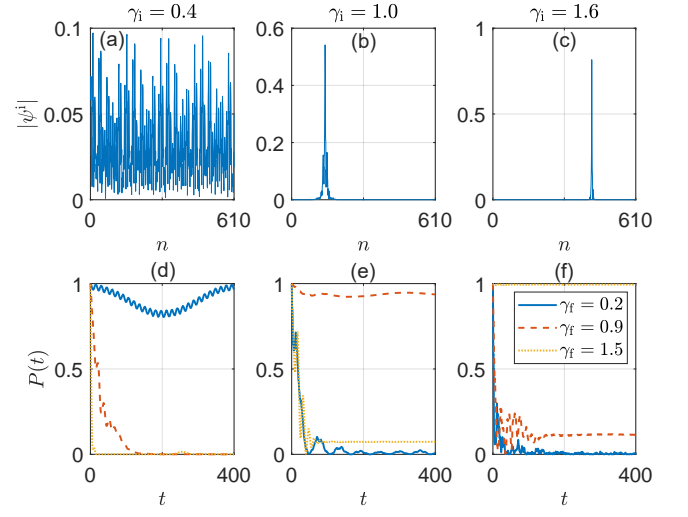


FIG. 11. Profiles of initial states [in (a)–(c)] and their return probabilities following quenches [in (d)–(f)] in the dimerized NHQC. The states in (a)–(c) are chosen to be the ones with the largest imaginary parts of energy at the corresponding phase shift γ_i . System parameters for (a)–(c) are set as $J = 1$, $V = 0.5$, $\Delta = 0.4$, $\alpha = \frac{\sqrt{5}-1}{2}$, and the length of lattice is $L = 610$ with PBC. In (d)–(f), the curves correspond to return probabilities of the initial states in (a)–(c) following quenches of γ from the corresponding γ_i to different values of γ_f applied at $t = 0$.

ized phases, as they both contain a sufficient amount of localized states to block the transport. One way to distinguish these two phases is by investigating the detailed profile of wavepackets during the evolution, as shown in Figs. 9(a)–(c). Another way is to consider the return probability of a state following quantum quenches [60], defined as $P(t) = |\langle \psi^i | \psi^f(t) \rangle|^2$, where the initial state $|\psi^i\rangle$ is an eigenstate of the prequench Hamiltonian \hat{H}^i , and $|\psi^f(t)\rangle$ is the final state evolved by the postquench Hamiltonian \hat{H}^f (not commute with \hat{H}^i) from $t = 0$ to t , i.e., $|\psi^f(t)\rangle = |\tilde{\psi}^f(t)\rangle \sqrt{\langle \tilde{\psi}^f(t) | \tilde{\psi}^f(t) \rangle}$ and $|\tilde{\psi}^f(t)\rangle = e^{-i\hat{H}^f t} |\psi^i\rangle$. For a given initial state, if the parameters of the pre and postquench Hamiltonians are set in phases with different localization nature, we expect the $P(t)$ to show qualitatively different behaviors. One can thus distinguish any two different phases of the system by investigating the wavepacket dynamics following a quench across the boundary between them. In our case, we choose the initial state to be an eigenstate of \hat{H} with $\gamma = \gamma_i$, and perform a quench at $t = 0$ by letting $\gamma_i \rightarrow \gamma_f$.

In Fig. 11, we show the return probabilities of initial states prepared in and quenched to different phases of the dimerized NHQC. In Fig. 11(a), the system is initialized in the extended phase with state profile $|\psi^i|$. When the postquench system is in the same phase, $P(t)$ undergoes oscillations without a global decay, as shown by the blue solid line in Fig. 11(d). If the postquench Hamiltonian is in the mobility edge phase, $P(t)$ is first subject to oscillations with a global decay profile, and approaches

zero in the long-time domain, as demonstrated by the red dashed line in Fig. 11(d). The initial oscillations of $P(t)$ can be traced back to the presence of extended states in the mobility edge phase. With the progress of time, the state is trapped by localized states in the mobility edge phase, leading to the decay of $P(t)$ at large t . If \hat{H}^f is in the localized phase, $P(t)$ decays very fast and quickly approaches zero, as depicted by the yellow dotted line in Fig. 11(d). Since all states are localized in the postquench system, the evolving state can never goes back. The distinctive features of $P(t)$ in three phases can thus help us to discriminate them following the postquench dynamics

if the initial state is prepared in the extended phase.

In Figs. 11(b) and 11(c), we prepare the system into a localized state in the mobility edge and insulator phases. The results in Figs. 11(e) and 11(f) suggest that the return probabilities also behave distinctly when \hat{H}^f is set in phases with different transport nature. Putting together, we conclude that wherever the initial state is prepared, its return probability following quenches to different phases could help us to distinguish them dynamically. In experiments, the averaged spreading velocity and return probability of wavepackets can thus be employed to detect phases with different localization nature in the dimerized NHQC.

-
- [1] Zilberberg O 2021 Optical Materials Express **11** 1592
 - [2] Jagannathan A 2020 arXiv:2012.14744 [cond-mat.stat-mech]
 - [3] Kramer B and Kinnon M A 1993 Rep. Prog. Phys. **56** 1469
 - [4] Sokoloff J B 1985 Phys. Rep. **126**, 189
 - [5] Aubry S and André G 1980 Ann. Israel Phys. Soc. **3**, 133
 - [6] Harper P G 1955 Proc. Phys. Soc. London A **68** 874
 - [7] Wang P, Zheng Y, Chen X, Huang C, Kartashov Y V, Torner L, Konotop V V, and Ye F 2020 Nature **577** 42
 - [8] Roati G, D'Errico C, Fallani L, Fattori M, Fort C, Zaccanti M, Modugno G, Modugno M, and Inguscio M 2008 Nature **453** 895
 - [9] Lüschen H P, Scherg S, Kohlert T, Schreiber M, Bordia P, Li X, Sarma S D, and Bloch I 2018 Phys. Rev. Lett. **120** 160404
 - [10] Lahini Y, Pugatch R, Pozzi F, Sorel M, Morandotti R, Davidson N, and Silberberg Y 2009 Phys. Rev. Lett. **103** 013901
 - [11] Ni X, Chen K, Weiner M, Apigo D J, Prodan C, Alù A, Prodan E, and Khanikaev A B 2019 Commun. Phys. **2** 55
 - [12] Levi L, Rechtsman M, Freedman B, Schwartz T, Manela O, and Segev M 2011 Science **332** 1541
 - [13] Vardeny Z V and Nahata A 2011 Nat. Photon. **5** 453
 - [14] Verbin M, Zilberberg O, Kraus Y E, Lahini Y, and Silberberg Y 2013 Phys. Rev. Lett. **110** 076403
 - [15] Kraus Y E, Lahini Y, Ringel Z, Verbin M, and Zilberberg O 2012 Phys. Rev. Lett. **109** 106402
 - [16] Lang L J, Cai X, and Chen S 2012 Phys. Rev. Lett. **108** 220401
 - [17] Ganeshan S, Sun K, and Sarma S D 2013 Phys. Rev. Lett. **110** 180403
 - [18] Cestari J C C, Foerster A, and Gusmao M A 2016 Phys. Rev. B **93** 205441
 - [19] Wang J, Liu X J, Gao X L, and Hu H 2016 Phys. Rev. B **93** 104504
 - [20] Liu F, Ghosh S, and Chong Y D 2015 Phys. Rev. B **91** 014108
 - [21] Zhou L, Wang H, Ho D Y H, and Gong J 2014 Eur. Phys. J. B **87** 204
 - [22] Sokoloff J B 1981 Phys. Rev. B **23** 6422
 - [23] Soukoulis C M and Economou E N 1982 Phys. Rev. Lett. **48** 1043
 - [24] Kohmoto M 1983 Phys. Rev. Lett. **51** 1198
 - [25] Thouless D J 1983 Phys. Rev. B **28** 4272
 - [26] Abe S and Hiramoto H 1987 Phys. Rev. A **36** 5349
 - [27] Guarneri I 1989 Europhys. Lett. **10** 95
 - [28] Geisel T, Ketzmerick R, and Petschel G 1991 Phys. Rev. Lett. **66** 1651
 - [29] Artuso R, Casati G and Shepelyansky D L 1992 Phys. Rev. Lett. **68** 3826
 - [30] Guarneri I and Mantica G 1994 Phys. Rev. Lett. **73** 3379
 - [31] Piechon F 1996 Phys. Rev. Lett. **76** 4372
 - [32] Wilkinson M and Austin E J 1994 Phys. Rev. B **50** 1420
 - [33] Ketzmerick R, Kruse K, Kraut S, and Geisel T 1997 Phys. Rev. Lett. **79** 1959
 - [34] Moura F A B F d and Lyra M L 1998 Phys. Rev. Lett. **81** 3735
 - [35] Jeon G S, Kim B J, Yiy S W, and Choi M Y 1998 J. Phys. A **31** 1353
 - [36] Boers D J, Goedeke B, Hinrichs D, and Holthaus M 2007 Phys. Rev. A **75** 063404
 - [37] Roscilde T 2008 Phys. Rev. A **77** 063605
 - [38] Roux G, Barthel T, McCulloch I P, Kollath C, Schollwöck U, and Giamarchi T 2008 Phys. Rev. A **78** 023628
 - [39] Schreiber A, Cassemiro K N, Potocek V, Gabris A, Jex I, and Silberhorn C 2011 Phys. Rev. Lett. **106** 180403
 - [40] Yao H, Khoudli H, Bresque L, and Sanchez-Palencia L 2019 Phys. Rev. Lett. **123** 070405
 - [41] Yao H, Giamarchi T, and Sanchez-Palencia L 2020 Phys. Rev. Lett. **125** 060401
 - [42] Jitomirskaya S Y 1999 Ann. Math. **150** 1159
 - [43] Avila A and Jitomirskaya S 2006 Lect. Notes Phys. **690** 5
 - [44] Rossignolo M and Dell'Anna L 2019 Phys. Rev. B **99** 054211
 - [45] Purkayastha A, Sanyal S, Dhar A, and Kulkarni M 2018 Phys. Rev. B **97** 174206
 - [46] Takada Y, Ino K, and Yamanaka M 2004 Phys. Rev. E **70** 066203
 - [47] Chang I, Ikezawa K, and Kohmoto M 1997 Phys. Rev. B **55** 12971
 - [48] Hiramoto H and Kohmoto M 1992 Int. J. Mod. Phys. B **06** 281
 - [49] Biddle J and Sarma S D 2010 Phys. Rev. Lett. **104** 070601
 - [50] Ganeshan S, Pixley J H, and Sarma S D 2015 Phys. Rev. Lett. **114** 146601
 - [51] Xu Z, Huangfu H, Zhang Y, and Chen S 2020 New J.

- Phys. **22** 013036
- [52] Longhi S 2019 Phys. Rev. Lett. **122** 237601
 - [53] Longhi S 2019 Phys. Rev. B **100** 125157
 - [54] Liu T, Guo H, Pu Y, and Longhi S 2020 Phys. Rev. B **102** 024205
 - [55] Longhi S 2021 Phys. Rev. B **103** 054203
 - [56] Jiang H, Lang L, Yang C, Zhu S, and Chen S 2019 Phys. Rev. B **100** 054301
 - [57] Liu Y, Jiang X P, Cao J, and Chen S 2020 Phys. Rev. B **101** 174205
 - [58] Liu Y, Wang Y, Zheng Z, and Chen S 2021 Phys. Rev. B **103** 134208
 - [59] Liu Y, Wang Y, Liu X, Zhou Q, and Chen S 2021 Phys. Rev. B **103** 014203
 - [60] Xu Z and Chen S 2021 Phys. Rev. A **103** 043325
 - [61] Zeng Q, Chen S, and Lü R 2017 Phys. Rev. A **95** 062118
 - [62] Cai X 2021 Phys. Rev. B **103** 014201
 - [63] Jazaeri A and Satija I I 2001 Phys. Rev. E **63** 036222
 - [64] Zeng Q, Yang Y, and Lü R 2020 Phys. Rev. B **101** 125418
 - [65] Zeng Q, Yang Y, and Xu Y 2020 Phys. Rev. B **101** 020201(R)
 - [66] Tang L, Zhang G, Zhang L, and Zhang D 2021 Phys. Rev. A **103** 033325
 - [67] Liu T, Cheng S, Guo H, and Gao X 2021 Phys. Rev. B **103** 104203
 - [68] Zhai L, Huang G, and Yin S 2021 Phys. Rev. B **104**, 014202
 - [69] Zeng Q and Xu Y 2020 Phys. Rev. Res. **2** 033052
 - [70] Su W, Schrieffer J, and Heeger A 1979 Phys. Rev. Lett. **42** 1698.
 - [71] Meier E J, An F A, Dauphin A, Maffei M, Massignan P, Hughes T L, and Gadway B 2018 Science **362** 929
 - [72] Asbóth J K, Oroszlány L, and Pályi A 2016 *A Short Course on Topological Insulators* (Cham: Springer) p. 1
 - [73] Ashida Y, Gong Z, and Ueda M 2020 Advances in Physics **69** 3
 - [74] Zhou L and Gong J 2018 Phys. Rev. B **98** 205417
 - [75] Zhou L, Wang Q, Wang H, and Gong J 2018 Phys. Rev. A **98** 022129
 - [76] Zykina A Y, Skryabin D V, and Kartashov Y V 2021 Opt. Lett. **46** 2123-2126
 - [77] Goldsheid I Y and Khoruzhenko B A 1998 Phys. Rev. Lett. **80** 2897
 - [78] Molinari L G 2009 J. Phys. A: Math. Theor. **42** 265204
 - [79] Markum H, Pullirsch R, and Wettig T 1999 Phys. Rev. Lett. **83** 484
 - [80] Chalker J T and Mehlig B 1998 Phys. Rev. Lett. **81** 3367
 - [81] Hamazaki R, Kawabata K, Kura N, and Ueda M 2020 Phys. Rev. Res. **2** 023286
 - [82] Girvin S M and Yang K 2019 *Modern Condensed Matter Physics* (Cambridge: Cambridge University Press) p. 255